Saturation effect in functional photoacoustic imaging

Jing Wang
University of Wisconsin-Milwaukee
Department of Electrical Engineering and Computer Science
3200 N Cramer Street
Milwaukee, Wisconsin 53201
and
Jilin University
College of Electronic Science and Engineering
2699 Qianjin Street
Changchun, Jilin 130012
China

Tan Liu
University of Wisconsin-Milwaukee
Department of Electrical Engineering and Computer Science
3200 N Cramer Street
Milwaukee, Wisconsin 53201

Shuliang Jiao
University of Southern California
Department of Ophthalmology
DOH 307E
Los Angeles, California 90033

Ruimin Chen
Qifa Zhou
K. Kirk Shung
University of Southern California
NIH Transducer Resource Center
and
Department of Biomedical Engineering
Los Angeles, California 90089

Lihong V. Wang
Washington University in St. Louis
Department of Biomedical Engineering
One Brooking Drive
St. Louis, Missouri 63130

Hao F. Zhang
University of Wisconsin-Milwaukee
Department of Electrical Engineering and Computer Science
3200 N Cramer Street
Milwaukee, Wisconsin 53201

Abstract. We investigate the saturation effect, which describes the violation of the linearity between the measured photoacoustic amplitude and the object's optical absorption coefficient in functional photoacoustic imaging when the optical absorption in the object increases. We model the optical energy deposition and photoacoustic signal generation and detection in a semi-infinite optical absorbing object. Experiments are carried out by measuring photoacoustic signals generated from an ink-filled plastic tube. The saturation effect is studied by varying the optical absorption coefficient in the model and the ink concentration in the photoacoustic experiments. By changing the center frequency of the ultrasonic detector, the requirement to minimize the saturation effect in functional photoacoustic imaging is established.
[DOI: 10.1117/1.3333549]

Keywords: photoacoustic imaging; functional imaging; saturation.

Paper 09323SSR received Jul. 31, 2009; revised manuscript received Dec. 11, 2009; accepted for publication Dec. 15, 2009; published online Mar. 11, 2010.

1 Introduction

Photoacoustic (PA) imaging is a novel hybrid imaging technology that is able to image in great depth the optical energy deposition with high spatial resolution in biological tissue.[1–3] Since optical energy deposition reflects the physiologically specific optical absorption contrast, PA imaging has been widely used to study various functional parameters of living biological tissue, especially hemoglobin oxygen saturation[4–7] (sO_2).

To measure sO_2, PA imaging depends on the difference in the molar extinction coefficient spectra of the two forms of hemoglobin, oxygenated hemoglobin (HbO_2) and deoxygenated hemoglobin (HbR). When a blood vessel is irradiated by laser pulses with identical pulse energy at different optical

Address all correspondence to: University of Wisconsin-Milwaukee, Department of Electrical Engineering and Computer Science, P.O. Box 784, Milwaukee, Wisconsin 53201. Tel: 414-229-1165; E-mail: zhang25@uwm.edu

1083-3668/2010/15(2)/021317/5/$25.00 © 2010 SPIE

wavelengths, PA signals are generated with different amplitudes due to the optical-wavelength-dependent molar extinction coefficients. Therefore, PA imaging performs spectral measurement and treats HbR and HbO_2 as the dominant optical absorbers at each wavelength (λ_i) to calculate their relative concentrations ([HbR] and [HbO_2], respectively) based on a least squares fit.[5] The sO_2 is further calculated by [HbO_2]/([HbO_2]+[HbR]).

The prerequisite for the aforementioned spectral measurement and inverse calculation (least-squares fit) is that the detected PA signals from blood are linearly related with the optical absorption coefficients of hemoglobin at λ_i, which denotes as the absorption-dependent PA detection. However, when the center frequency of the ultrasonic detector is low with respect to the corresponding optical absorption coefficient,[8] the detected PA signal will not linearly reflect the optical absorption change in blood. In an extreme case, the detected PA signal may rely on only the incident optical energy regardless of the optical absorption coefficient of blood. This phenomenon is referred to as the saturation effect.[9] When saturation effect occurs, the inverse calculation of the [Hb] and [HbO_2] becomes inaccurate.

In the *in vivo* PA imaging of sO_2, the required maximum imaging depth for different applications varies from a few hundred micrometers to several millimeters. In general, increased maximum imaging depth requires the ultrasonic detector to have a lower center frequency because of the wavelength-dependent ultrasonic attenuation in tissue.[10] Due to the saturation effect, however, a threshold of the ultrasonic center frequency could exist. Using an ultrasonic detector with a center frequency below such a threshold will lead to saturation in the PA signal detection and present an incorrect inverse calculation of sO_2 with an error greater than a preset value.

Here, we report both the theoretical and experimental studies of the saturation effect in functional PA imaging. In our experiments, the change of the optical absorption coefficient was achieved by varying the concentration of the optical absorbing material rather than the optical wavelength. The saturation effect discussed here is limited to the nonlinear dependency of the measured PA amplitude with the optical energy deposition under the adiabatic heating condition induced by short laser pulses. Other nonlinear effects caused by, for example, heat diffusion[11] are excluded.

2 Methods and Materials

We used a semi-infinite homogeneous optical absorbing object, as shown in Fig. 1, to model the optical energy deposition as well as the PA wave generation and detection. This model is valid as an approximation for blood vessels when the optical penetration depth is less than one-tenth of the vessel diameter. Within the spectral range of 520 to 600 nm, the optical absorption coefficient of the whole blood (considering the sO_2 to be 95%) is[12] 20 to 296 cm^{-1}, corresponding to a penetration depth of 34 to 491 μm. In our model, the laser illumination is along the z axis and the ultrasonic detector is placed directly above the illuminated area.

The depth-resolved optical fluence distribution $F(z)$ inside the object is described as

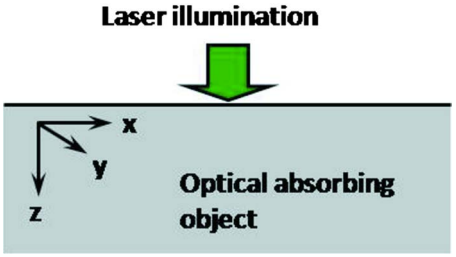

Fig. 1 Semi-infinite optical absorbing object to model optical energy deposition and PA signal generation.

$$F(z,\mu_a) = F_0 \exp(-\mu_a z), \tag{1}$$

where F_0 (in joules per squared centimeter) is the optical fluence on the surface of the object, and μ_a (in inverse centimeters) is the optical absorption coefficient of the medium. Hence, the induced depth-resolved PA waves can be described as

$$\mathrm{PA}(z,\mu_a) = F_0 k_1 \mu_a \exp(-\mu_a z), \tag{2}$$

where k_1 is the conversion coefficient of the PA effect (dimensionless), which is the result of the Grueneisen parameter (dimensionless) multiplied by the percentage of optical energy deposition that is converted to heat.[13]

As the peak amplitude of the detected PA signals is usually taken as a measure of the optical energy deposition in a vessel, here we estimate the peak amplitude of the detected PA signal for Eq. (2). If an ultrasonic detector has an infinitely high axial resolution, the detected peak PA amplitude will be $\alpha F_0 k_1 \mu_a$, where α is the coefficient of the ultrasonic detection system that converts pressure to voltage. For an ultrasonic detection system that has only finite axial resolution, the detected PA signal is an integration of the PA waves within a specific axial pixel. For a given wideband ultrasonic detector at a cut-off wavelength of λ_c, the axial resolution in PA imaging can be approximated[14] as $k_2\lambda_c$, where k_2 is a dimensionless coefficient between 0.8 to 0.92. Thus, the detected PA peak amplitude can be approximated as

$$\begin{aligned} A_{\mathrm{PA}}(\mu_a) &= \alpha \int_0^{k_2\lambda_c} F_0 k_1 \mu_a \exp(-\mu_a z)\mathrm{d}z \\ &= \alpha F_0 k_1 [1 - \exp(-\mu_a k_2 \lambda_c)]. \end{aligned} \tag{3}$$

The experiments were carried out by measuring PA peak-to-peak amplitudes detected from an ink (Fiesta Red, Private Reserve Ink, The Ink Flow, San Antonio, Texas) filled plastic tube (Tygon® S-54-HL Microbore Tubing 56464, United States Plastic Corp., Lima, Ohio). The measured optical absorption spectrum of the ink is shown in Fig. 2. The optical wavelength used for the PA measurement was 523 nm. The corresponding optical absorption coefficient was 1028 cm^{-1}. The tube has an inner diameter of 0.5 mm and an outer diameter of 1.5 mm.

A schematic diagram of the experimental setup is shown in Fig. 3. Laser light at 523 nm was generated by a Nd:YLF laser (INNOSLAB; IS8II-E; EdgeWave, Germany). The pulse width was 6 ns, the pulse repetition was set to 100 Hz, and the laser beam diameter was 10 mm. The light coming out of

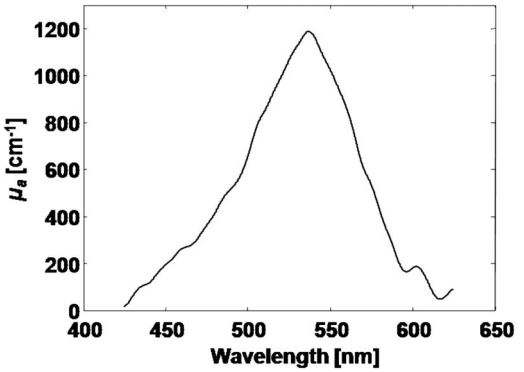

Fig. 2 Measured optical absorption spectrum of the red ink at 100% concentration.

the laser first passed through a beam sampler, then a right-angle prism (PS908; Thorlabs, Newton, New Jersey), and finally a neutral density filter (NE10A; optical density: 1.0; Thorlabs, Newton, New Jersey) before it illuminated the tube. The light was attenuated because of better pulse energy stability when the laser system is working at a higher driving current.

The PA waves were detected by a high-frequency, unfocused ultrasonic transducer and amplified by a wideband, lownoise preamplifier (ZFL500LN+, Mini-Circuits, Brooklyn, New York) for 28 dB. The amplified PA signals were then digitized and stored by an oscilloscope (TDS5034B, Tektronix, Beaverton, Oregon). A fast photodiode (DET10A, Thorlabs, Newton, New Jersey) detected the sampled laser pulses to generate triggers for data acquisition. Each PA signal was averaged 600 times to minimize the influence from the pulse energy instability.

Three ultrasonic detectors were used in the experiments. Their respective center frequencies and bandwidths (−6 dB) were 10 and 9 MHz (V312, Olympus, Waltham, Massachusetts), 20 and 10 MHz (V317, Olympus, Waltham, Massachusetts), and 40 and 15 MHz [custom-built by the National Institutes of Health (NIH) Resource Center for Medical Ultrasonic Transducer Technology,[15,16] The University of Southern California, Los Angeles]. Their corresponding cutoff wavelengths were 105, 60, and 32 μm. Each transducer was positioned independently to reach its maximum PA amplitude.

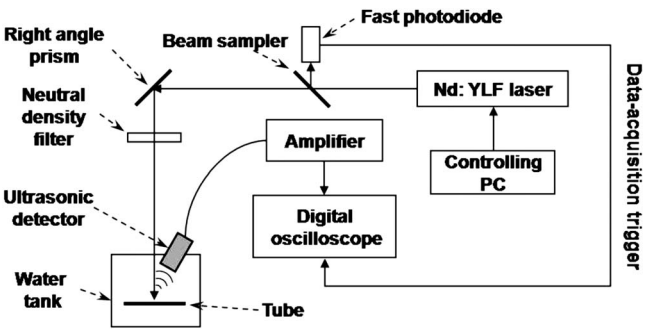

Fig. 3 Schematic of the experimental setup.

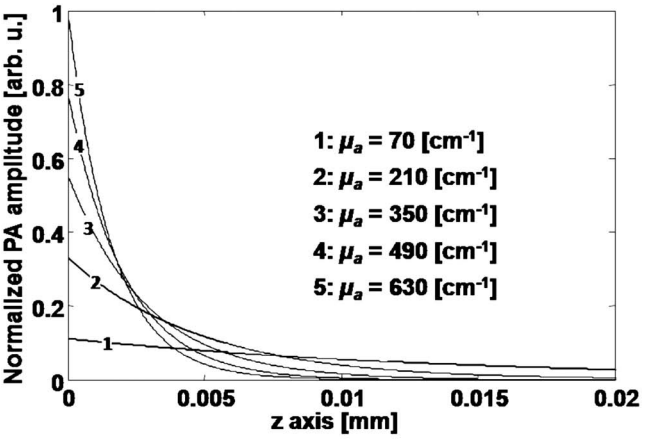

(a)

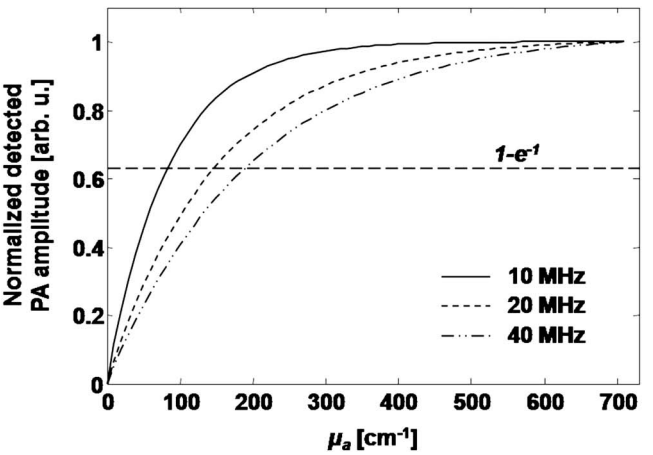

(b)

Fig. 4 Theoretical study of the PA pressure and the detected PA amplitude: (a) depth-resolved PA pressure induced by a delta laser pulse illumination in media with different optical absorption coefficients and (b) correlation of the detected PA peak amplitude with μ_a detected by different ultrasonic detectors.

3 Results and Discussions

Figure 4 gives the theoretical calculations of PA(z,μ_a) and $A_{\mathrm{PA}}(\mu_a)$. Figure 4(a) shows the normalized depth-resolved PA waves along the z axis in the semi-infinite object calculated from Eq. (2). The μ_a was varied from 70 to 630 cm^{-1} with a step size of 140 cm^{-1}. For simplicity, all the PA(z,μ_a) were normalized by $F_0 k_1 \mu_{a\,\max}$, where $\mu_{a\,\max}$ is the maximum value of μ_a used in simulation study, which was 720 cm^{-1}. As we can see in Fig. 4(a), higher μ_a induces larger PA pressure peak amplitude under the same optical illumination, but the depth-resolved signal decays faster than those with lower μ_a values.

When an ultrasonic detector measures the induced PA pressures for anatomical or functional imaging purposes, a time-resolved PA signal will be acquired. In most situations, the peak-to-peak amplitude of the detected PA signal is used to measure functional parameters such as sO_2. Ideally, the detected PA signal is anticipated to be identical with the induced PA pressures inside the sample; however, because ultrasonic detection is band-limited and thus has only limited axial res-

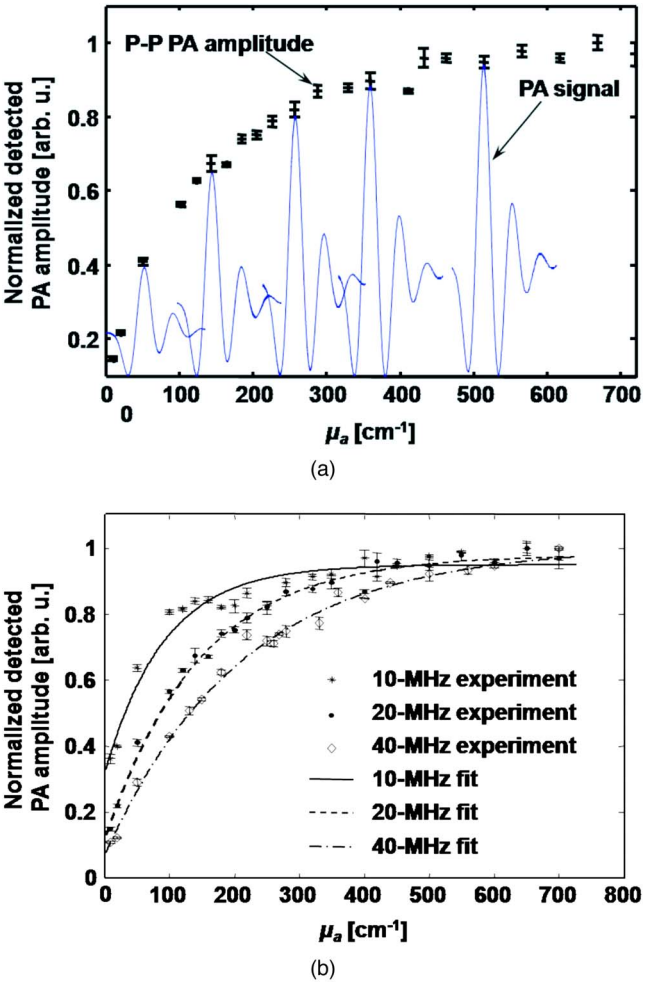

Fig. 5 Experimental study of the saturation effect in ink phantoms: (a) detected PA amplitudes acquired from various ink concentrations using the 20-MHz detector, the temporal profiles of the PA signals measured at ink concentrations of 5, 15, 28, 36, and 50% are plotted at their corresponding μ_a values, and (b) correlation between the detected PA peak amplitude μ_a of the ink phantom for different ultrasonic center frequencies. P-P, peak-to-peak.

olution, the detected PA signal must be integrated within an ultrasonically resolvable depth. Such resolvable depth can be considered as the axial resolution and is related with the ultrasonic center frequency and bandwidth.[10,14] In our work, the axial resolution is approximated by $k_2\lambda_c$.

Figure 4(b) shows the calculated $A_{\mathrm{PA}}(\mu_a)$ for the three ultrasonic detectors used in the experiments. In the simulation, k_2 was set to 0.92 and the $A_{\mathrm{PA}}(\mu_a)$ for each ultrasonic center frequency was normalized independently. As we can observe in Fig. 4(b), when μ_a is low, $A_{\mathrm{PA}}(\mu_a)$ increases proportional to μ_a for all three center frequencies; however, when μ_a is higher than a certain value, the correlation between μ_a and $A_{\mathrm{PA}}(\mu_a)$ loses its linearity and eventually reaches a plateau, which demonstrates the saturation effect. Moreover, the nonlinearity becomes more severe when the ultrasonic center frequency lowers. In Fig. 4(b), the PA signal detected by a 10-MHz ultrasonic detector was saturated at a μ_a value lower than those detected by 20- and 40-MHz ultrasonic detectors. If we consider the μ_a value corresponding with the $1/e$ decay of $A_{\mathrm{PA}}(\mu_a)$ as the "turn point" of the saturation, the linear range for a given λ_c can be found from the simulation results. As seen in Fig. 4(b), the horizontal line corresponding with the value of $1-e^{-1}$, where the left side of the cross point with each $A_{\mathrm{PA}}(\mu_a)$ representing the preferred linear measuring range. It is important to understand that such a transition at the $1/e$ "turn point" between linearity and saturation is not abrupt.

The saturation effect limits the selection of the ultrasonic detector's center frequency and bandwidth in functional PA imaging since the inverse calculation of sO_2 requires the $A_{\mathrm{PA}}(\mu_a)$ to be linearly associated with optical absorption. Due to the dramatic variation in the molar excitation coefficients of Hb and HbO_2 within the spectral range of 520 to 600 nm, the PA measurement may be saturated within a certain spectral range while remaining linear within others. The saturation effect was further observed by measuring PA signals generated from the ink phantoms. The same normalization scheme as that used for Fig. 4(b) was used in the experiments.

Figure 5(a) shows the change of the detected PA amplitude using the 20-MHz ultrasonic detector when the ink concentration increases. The temporal profiles of several detected PA waves are also shown in the Fig. 5(a). Similar temporal shapes can be observed for PA waves within both the linear and saturated ranges. As shown in Fig. 5(b), the experimental data acquired from three ultrasonic detectors demonstrate the same trend as that in the simulation results, where the saturation starts much earlier for the 10-MHz transducer than transducers with higher center frequencies.

We further fit the experimental data to verify k_2. The target fitting function was simplified from Eq. (3) to be a-b $(e^{-c\mu_a})$, where a, b, and c are unknown constants. After fitting was conducted for all three ultrasonic transducers, we acquired $a=0.98\pm0.016$, $b=0.82\pm0.090$, and $c=0.0076\pm0.0018$. Then k_2 was subsequently calculated to be 1.15 ± 0.10. Compared with the values reported in Ref. 14, our value is only slightly higher, possibly due to experimental noises and different optical-ultrasonic geometry. Both the simulation and experimental results indicate that the ultrasonic detector used for functional PA imaging should satisfy $k_2\lambda_c\mu_a \leqslant 1$ to avoid saturation. In this situation, Eq. (3) becomes $A_{\mathrm{PA}}(\mu_a) = \alpha F_0 k_1 k_2 \lambda_c \mu_a$ by ignoring high-order terms in the Taylor expansion.

4 Summary

We have used a semi-infinite homogeneous optical absorbing medium to model laser-induced, depth-resolved PA pressure and the resolution-limited detected PA amplitude. The saturation effect was simulated by varying the optical absorption coefficient of the medium. The saturation effect was further observed in ink phantoms using three ultrasonic detectors with center frequencies of 10, 20, and 40 MHz. The experimental results agreed with the theoretical studies and the fitted constant agrees with the reported theoretical estimation.

Acknowledgments

This work was supported in part by start-up funding from the University of Wisconsin-Milwaukee, a grant from The Lynde and Harry Bradley Foundation, and financial support from the Chinese Ministry of Education to J. Wang.

References

1. A. A. Oraevsky and A. A. Karabutov, "Optoacoustic tomography," Chap. 34 in *Biomedical Photonics Handbook*, T. Vo-Dinh, Ed., Vol. **PM125**, CRC Press, Boca Raton, FL (2003).
2. L. V. Wang, "Tutorial on photoacoustic microscopy and computed tomography," *J. Select. Top. Quantum Electron.* **14**, 171–179 (2008).
3. X. Wang, Y. Pang, G. Ku, X. Xie, G. Stoica, and L. V. Wang, "Noninvasive laser-induced photoacoustic tomography for structural and functional *in vivo* imaging of the brain," *Nature Biotechnol.* **21**, 803–806 (2003).
4. H. F. Zhang, K. Maslov, G. Stoica, and L. V. Wang, "Functional photoacoustic microscopy for high-resolution and noninvasive *in vivo* imaging," *Nature Biotechnol.* **24**, 848–851 (2006).
5. H. F. Zhang, K. Maslov, M. Sivaramakrishnan, G. Stoica, and L. V. Wang, "Imaging of hemoglobin oxygen saturation variations in single vessels *in vivo* using photoacoustic microscopy," *Appl. Phys. Lett.* **90**, 053901 (2007).
6. J. G. Laufer, D. T. Delpy, C. E. Elwell, and P. C. Beard, "Quantitative spatially resolved measurement of tissue chromophore concentrations using photoacoustic spectroscopy: application to the measurement of blood oxygenation and haemoglobin concentration," *Phys. Med. Biol.* **52**, 141—168 (2007).
7. Y. Wang and R. K. Wang, "Photoacoustic recovery of an absolute optical absorption coefficient with an exact solution of a wave equation," *Phys. Med. Biol.* **53**, 6167–6177 (2008).
8. K. Maslov, H. F. Zhang, and L. V. Wang, "Effects of wavelength-dependent fluence attenuation on the noninvasive photoacoustic imaging of hemoglobin oxygen saturation in subcutaneous vasculature *in vivo*," *Inverse Probl.* **23**, S113–S122 (2007).
9. M. Sivaramakrishnan, K. Maslov, H. F. Zhang, G. Stoica, and L. V. Wang, "Limitations of quantitative photoacoustic measurement of blood oxygenation in small vessels," *Phys. Med. Biol.* **52**, 1349–1361 (2007).
10. H. F. Zhang, K. Maslov, and L. V. Wang, "*In vivo* imaging of subcutaneous structures using functional photoacoustic microscopy," *Nature Proto.* **2**, 797–804 (2007).
11. I. G. Calasso, W. Craig, and G. J. Diebold, "Photoacoustic point source," *Phys. Rev. Lett.* **86**, 3550–3553 (2001).
12. S. Prahl, "Optical Absorption of Hemoglobin," http://omlc.ogi.edu/spectra/hemoglobin/index.html.
13. L. V. Wang and H.-I. Wu, Eds., "Photoacoustic tomography," Chap. 12 in *Biomedical Optics: Principles and Imaging*, pp. 283–321, Wiley, Hoboken, NJ (2007).
14. M. Xu and L. V. Wang, "Photoacoustic imaging in biomedicine," *Rev. Sci. Instrum.* **77**, 041101 (2006).
15. Q. F. Zhou, X. Xu, E. Gottlieb, L. Sun, J. Cannata, H. Ameri, M. Humayun, P. D. Han, and K. K. Shung, "PMN-PT single crystal high frequency ultrasonic needle transducers for pulsed wave Doppler application," *IEEE Trans. Ultrasons. Ferroelectr. Freq. Control* **54**, 668–675 (2007).
16. Q. Zhou, D. Wu, J. Jin, C.-H. Hu, X. Xu, J. Williams, J. Cannata, L. C. Lim, and K. K. Shung, "Design and fabrication of PZN-7%PT single crystal high frequency angled needle ultrasound transducers," *IEEE Trans. Ultrason. Ferroelectr. Freq. Control* **55**, 1394–1399 (2008).